

***Ab initio* theoretical studies on photodissociation of HNCO upon $S_1(1A'') \leftarrow S_0(1A')$ excitation: The role of internal conversion and intersystem crossing**

Alexey L. Kaledin, Qiang Cui, Michael C. Heaven, and Keiji Morokuma

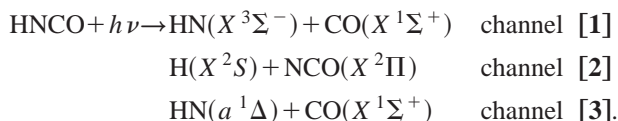
Cherry L. Emerson Center for Scientific Computation and Department of Chemistry, Emory University, Atlanta, Georgia 30322

(Received 1 March 1999; accepted 23 June 1999)

Photodissociation of isocyanic acid, HNCO, was studied with high-level *ab initio* methods. Geometry optimizations of stationary points and surface crossing seams were performed with the complete active space self-consistent-field (CASSCF) method, and the energetics were re-evaluated with single-point second-order multireference perturbation theory (CASPT2). The three product channels that participate in the photodissociation process are [1] $\text{HN}(X^3\Sigma^-) + \text{CO}$ at 86.0 (calculated 79.6) kcal/mol, [2] $\text{H} + \text{NCO}(X^2\Pi)$ at 109.7 (108.7) kcal/mol, and [3] $\text{HN}(a^1\Delta) + \text{CO}$ at 122.2 (120.8) kcal/mol. The four electronic states, S_0 , S_1 , T_1 , and T_2 , that interconnect these channels were studied in detail. S_1 exhibits dissociation barriers to both, channel [2] and [3], whose respective reverse heights are 11.3 and 1.2 kcal/mol, in good agreement with experiment as well as previous theoretical works. The two triplets, T_1 and T_2 , show barriers of similar heights for HN bond fission, while S_0 has no barriers to either channel. Various key isomerization transition states as well as numerous minima on the seam of surface crossings (MSX's) were also found. At photoexcitation energies near channel [3] threshold, products to channel [3] are likely to be formed via $S_1 \rightarrow [3]$ (if enough energy in excitation) and $S_1 \rightarrow S_0 \rightarrow [3]$. Channel [2] can be formed via $S_1 \rightarrow S_0 \rightarrow [2]$; (HN-mode quanta) + $S_1 \rightarrow T_1 \rightarrow [2]$; $S_1 \rightarrow T_2 \rightarrow [2]$; $S_1 \rightarrow T_2 \rightarrow T_1 \rightarrow [2]$, and channel [1] via $S_1 \rightarrow S_0 \rightarrow T_1 \rightarrow [1]$, $S_1 \rightarrow T_1 \rightarrow [1]$ and $S_1 \rightarrow T_2 \rightarrow T_1 \rightarrow [1]$. At higher photoexcitation energies the $S_1 \rightarrow [3]$ pathway is expected to be dominant while $S_1 \rightarrow [2]$, with the higher activation energy, is expected to drop rapidly. Also addressed are such important issues as the impact of a vibrationally excited HN mode on a channel [2] yield, and the band origin of the $S_1 \leftarrow S_0$ excitation spectrum. © 1999 American Institute of Physics. [S0021-9606(99)30535-3]

I. INTRODUCTION

The unimolecular decomposition of HNCO has been studied extensively in the past. The photochemistry of HNCO is especially interesting because of the low-lying optically accessible excited state¹⁻¹⁹ and a high density of states in the excited state region.^{20,21} Several dissociation channels become available upon photoexcitation of the system as they become involved in a complex dissociation dynamics.^{22,23} Such state-of-the-art techniques as photofragment imaging have been successfully employed to study the dynamics of the system.^{22,24} In these experiments it was found that three different channels compete for dissociation, and this competition is strongly dependent upon the excitation wavelength. These channels are



In UV experiments Reisler and co-workers established that at excitation wavelengths in the region of 119.23–130.09 kcal/mol (240–220 nm) the dominant dissociation channel is $\text{H}(X^2S) + \text{NCO}(X^2\Pi)$, channel [2], with the threshold of 109.7 kcal/mol.²² As the excitation energy increased, the yield to channel [2] diminished at the cost of a

growing yield to channel [3] products, $\text{HN}(a^1\Delta) + \text{CO}(X^1\Sigma^+)$. At energies just exceeding 122.2 kcal/mol, the yield to channel [3] is very small compared to that of channel [2]. The yield to channel [3] becomes appreciable and, eventually, dominant only when the photon energy has substantially exceeded 122.2 kcal/mol. The product recoil anisotropy is much weaker for excitation energies just exceeding the threshold than it is for higher energies. This observation suggests that the two electronic surfaces, S_0 and S_1 are competing for dissociation, and there exists a very low barrier on S_1 , of the order of 1–2 kcal/mol. S_0 , on the other hand, is proposed to be barrierless. Furthermore, Reisler and co-workers reported a relatively small constant yield to channel [1] at a wide range of excitation wavelengths. Channel [1] is accessible after the spin-forbidden transition from S_1 to T_1 .

Parallel experiments of Crim and co-workers also investigated the photodissociation mechanism of HNCO to the three main channels.^{2,25} There is a perfect agreement between the two groups on the thresholds to channels [2] and [3] and an overall agreement on the global photodissociation process. But the main focus of Crim's group has been on understanding mode-selective dissociation dynamics to channel [2]. Given several vibrational quanta in the H–N mode with the total energy of 124.3 kcal/mol, the consequent H–N

bond fission appears much more efficient (about 4 times) than that of an unexcited H–N stretch with the same total energy.

There exist several extensive theoretical studies of HNCO. A most exhaustive set of calculations was previously carried out by Mebel *et al.* in our group.²⁶ The entire potential energy surfaces (PES's) for the ground S_0 and the first triplet T_1 state were explored, and numerous minima and transition states for isomerization and dissociation were found. An exit barrier on the T_1 surface to $\text{HN}({}^3\Sigma^-) + \text{CO}({}^1\Sigma^+)$ products was found, and also a crossing between S_0 and T_1 was located. The exit barrier on the T_1 surface to $\text{H} + \text{NCO}({}^2\Pi)$ channel was shown to be high in energy. Another theoretical work by Fang *et al.*²⁷ also concentrated on the triplet dissociation pathway. The authors explicitly considered spin–orbit interaction between S_0 , and T_1 . It was shown that spin–orbit coupling is very important for the ground state dissociation into the $\text{HN}({}^3\Sigma^-) + \text{CO}({}^1\Sigma^+)$ products at high temperature. The first excited singlet, S_1 , was also discussed.

Since the first excited singlet, S_1 , is the only optically accessible electronic state in the dissociation threshold region, the initial system dynamics will occur on this state. Early works, such as those of East and Allen,^{21,28} considered vertical excitations to S_1 from S_0 in the Franck–Condon region. Small-scale CASSCF methods were used to predict excitation energies and to locate stable structures on S_1 .

More rigorous work on S_1 was performed quite recently by Stevens *et al.* in our group.²⁹ Using CASSCF (12e/10o)/DZP geometry optimization followed by CASPT2 and MRSDCI/DZP single point calculations, the geometries and energies of the intermediates, transition states, and products on S_1 were calculated. It was concluded that there existed a low, 500–600 cm^{-1} , reverse barrier on S_1 to the $\text{HN}({}^1\Delta) + \text{CO}({}^1\Sigma^+)$ exit channel. The S_1 barriers to the less endothermic $\text{H} + \text{NCO}({}^2\Pi)$ channel were found to be much higher in energy. Klossika *et al.*³⁰ used the MRSDCI/TZP method with a (10e/9o) reference space to map a 3D S_1 PES. This reference space was supposed to exclude the lone pairs and CO's σ and σ^* orbitals, and a reference selection threshold 0.05 of CI coefficient was applied. However, the authors mentioned that the PES was not smooth at certain regions, and this was probably the consequence of inconsistent active and reference configuration spaces. Nonetheless, their results are quantitative in some regions, and their calculated reverse barrier of 550 cm^{-1} to $\text{HN}({}^1\Delta) + \text{CO}({}^1\Sigma^+)$ exit channel agrees very well with the available experimental value.

As suggested by experiments, several electronic states are involved in the dissociation dynamics following excitation. The strongest competition is believed to take place for S_0/S_1 surfaces when photon energy has just exceeded channel [3] threshold.²² Another competition is suggested to involve the S_1/T_1 and S_0/T_1 pairs for dissociation to channel [1].^{22,25} Although not observed directly, the other triplet, T_2 , can also participate in the dissociative process.²² None of the above theoretical studies addressed extensively to the nonadiabatic transitions between various states.

In addition, the questions of initial excitation, $S_1 \leftarrow S_0$,

and the band origin of the absorption spectrum still remain partially unanswered.^{29,31} Disagreement between theory and experiment on the band origin (lowest energy transition) was attributed by Stevens *et al.*²⁹ to strongly nonvertical nature of the excitation. They also indicated the system's preference towards *trans* geometries immediately following the one-photon absorption, based on the calculated electronic dipole transition moment as a function of nuclear coordinates, although the vibrational wave function may also strongly influence the electronic transition.

Thus, the objectives of this work include the following: (a) to accurately describe the topology of S_0 , S_1 , T_1 , and T_2 electronic state PES's; (b) to investigate S_0/S_1 and T_1/T_2 internal conversions (IC) and S_i/T_j intersystem crossings (ISC); (c) to investigate the band origin and the nature of initial excitation, $S_1 \leftarrow S_0$; and (d) to build a qualitative picture of the global photodissociation dynamics as a competitive process between the three exit channels involving multiple PES's.

II. METHODS OF CALCULATION

We use the Dunning double zeta basis set with a set of *d*-polarization functions on the heavy elements with exponents 0.75 (C), 0.8 (N), and 0.85 (O), respectively, and a set of *p*-polarization functions on hydrogen with exponent 1.0.³² This basis was augmented with a set of diffuse *s* and *p* functions on C, N, and O with exponents 0.0438, 0.0639, and 0.0845, respectively, and a diffuse *s* function of hydrogen with exponent 0.036.³³

For geometry optimizations of stationary points on the five-dimensional HNCO hypersurface (constrained to planarity) and for qualitative energetics, we used the complete active space self-consistent-field (CASSCF) method.³⁴ For several critical planar structures, the energy was tested numerically with respect to small changes in the torsion angle. The present CASSCF calculations are all state-specific and C_s symmetry constrained unless noted otherwise.

The largest CASSCF active space we used consisted of all the valence orbitals except the 2*s* lone pair of oxygen. Hence, 14 electrons were distributed among 12 molecular orbitals resulting, on the average, in $\sim 85\,000$ configuration state functions. This nearly full valence (14e/12o) active space proved to be totally consistent throughout the entire PES, even in the asymptotic region, and therefore should be a qualitatively reliable reference for a dynamically correlated calculation. As a check for consistency we performed calculations on the products separately and in the supermolecule approach. The resulting geometries and energies came out to be identical. A smaller active space (12e/10o) was also used in the present calculations. Qualitatively, (12e/10o) excludes the CO (σ, σ^*) pair. The expense of CASSCF(12e/10o) was much smaller than that of CASSCF(14e/12o), so that approximate stationary points were always located first with this small active space, and later all the structures were re-optimized with CASSCF(14e/12o) and labeled as "CASSCF" throughout the paper unless noted otherwise.

To recover the dynamical correlation, we performed single point calculations with the internally contracted multireference second-order perturbation theory (CASPT2).³⁵

TABLE I. Energies of dissociation limits (in kcal/mol, with respect to the minimum on the ground state, S_0 TM), calculated with various methods and taken from references.

Method Channel	Method											
	CASSCF	PT2-FV	PT2-86	PT2-FV //PT2-86	EOMCC w.ZPE	EOMCC w.ZPE	MRSDCI Ref. 29	B3LYP Ref. 26	B3LYP w.ZPE Ref. 26	UMP2 Ref. 27	CASSCF Ref. 29	Expt. Ref. 42
[1]	64.3	77.8	77.6	79.6	72.8	67.1		93.9	88.3	90.0		86.0
[2]	99.8	108.4	99.8	108.7	109.14	101.8	109.4	113.5	105.5		101.0	109.7
[3]	109.9	119.6	117.9	120.8			123.7			110.8	96.9	122.2

Two reference spaces used for CASPT2 were the (14e/12o) active space described above, and a (10e/9o), which is (14e/12o) excluding 2s lone pair on nitrogen and σ and σ^* of CO. Both reference spaces were constructed from the same CASSCF(14e/12o) orbitals and gave very similar energetics. All electrons except the core and the 2s lone pair of oxygen were correlated in the CASPT2. This method with the (10e/9o) reference space will be referred to as “PT2-FV.” These correlated calculations are also assumed to be constrained to C_s unless stated otherwise.

Since only numerical gradient with CASPT2 was available, we used an additional small reference to perform geometry optimizations with CASPT2. That reference consisted of only 8 electrons in 6 orbitals, and the resulting method is labeled “PT2-86.” The consistency of PT2-86 energies depends on the consistency of the (8e/6o) active space, which, in turn, is very much dependent on geometry. We found that the (8e/6o) active space is pathologically inconsistent on going from one region on the potential energy surface to another, and this inconsistency is most pronounced near dissociation. In other words, if we scanned a dissociation path along some coordinate, we would face a discontinuity of several kcal/mol in the energy curve. Thus, we have to be cautious about PT2-86 energetics. However, the optimized geometries are less prone to be affected by the active space, and we define another version, labeled “PT2-FV//PT2-86” of single point CASPT2 energies at the PT2-FV level for the PT2-86 optimized geometries, which is our best estimate of single point energy. Unfortunately, PT2-FV and PT2-FV//PT2-86 calculations proved to be too memory—and time-demanding for all triplets and some structures on single surfaces. We report these energetics for most of the important structures, and hope that PT2-86 energy will mimic the higher level methods for the rest of the structures.

In the special case of nonplanar geometries, i.e., for C_1 symmetry, we used CCSD³⁶ and EOM-CCSD³⁷ methods in part because of the greatly increased computational cost for CASPT2. Additional difficulties were caused by convergence problems in CASSCF. However, we managed to calculate C_1 geometries with CASPT2 for very small displacements out of plane for the purposes of checking out-of-plane stability. For the regions on S_0 with HN or CN bonds elongated as compared to the global minimum structure, we used two-determinant reference for CCSD to account for the open-shell singlet character. We used these coupled-cluster techniques mainly for vibrational analysis in the Franck–Condon region and for determination of surface crossings, as will be discussed later.

In order to obtain dissociation transition states with the dynamically correlated PT2-FV and PT2-86 levels where the gradient is not available, we used a “walking” technique, assuming that the distance of the bond being broken is the reaction coordinate. Although this technique could in general lead to a false transition state or reaction pathway,³⁸ it should be acceptable for dissociation pathway where the reaction coordinate clearly remains to be this bond distance. We performed such calculations by optimizing the other coordinates with PT2-86 and obtaining single point energies with PT2-FV and PT2-86 for a few selected dissociation transition states.

The electronic structure method described above, coupled with the D95++(*d,p*) basis, is not of spectroscopic quality but should give a qualitative picture of HNCO potential energy surfaces. *Ab initio* quantum chemistry packages MOLPRO96.4,³⁹ GAMESS96,⁴⁰ and ACESII⁴¹ were used to perform calculations in this study.

III. RESULTS

Before results are presented, we need to define a spectroscopic notation for the electronic states of interest. The ground electronic state, $1^1A'$ (in C_s , 1^1A in C_1), is referred to as S_0 , and the first singlet excited state $1^1A''$ (2^1A) is referred to as S_1 . The lowest triplet, $1^3A''$ (1^3A), is referred to as T_1 , while the $1^3A'$ (2^3A) is labeled T_2 . There is, however, an ambiguity associated with this notation, namely, in the case of symmetry-allowed conical intersections. In the C_s plane, for example, S_0 is allowed to cross S_1 , and T_1 is allowed to cross T_2 , but as soon as the symmetry is lowered to C_1 , the degeneracy is lifted, and the electronic state in C_1 symmetry changes character from S_0 to S_1 or T_1 to T_2 . This certainly complicates the picture, but unless we specifically mention any conical intersection, we assume the above C_s -based notation.

Dissociation products, or channels, are labeled, as shown in Introduction, simply according to their energy. Thus, the lowest energy channel $\text{HN}(X^3\Sigma^-) + \text{CO}(X^1\Sigma^+)$, is channel [1], whose energy relative to the global minimum is ~ 78 kcal/mol in PT2-FV vs experimental value of 86 kcal/mol. The next lowest dissociation channel [2], $\text{H} + \text{NCO}(X^2\Pi)$, has the PT2-FV energy of ~ 108 kcal/mol vs that of experiment of ~ 110 kcal/mol. The next dissociation channel, [3], $\text{HN}(a^1\Delta) + \text{CO}$, has a relative energy of ~ 120 kcal/mol at PT2-FV vs experimental estimate of ~ 122 kcal/mol. The above experimental values for dissociation energies are taken from Ref. 42. Implicitly considered is another dissociation limit, $\text{HN}(A^3\Pi) + \text{CO}$. Table I and Fig. 1 summarize the

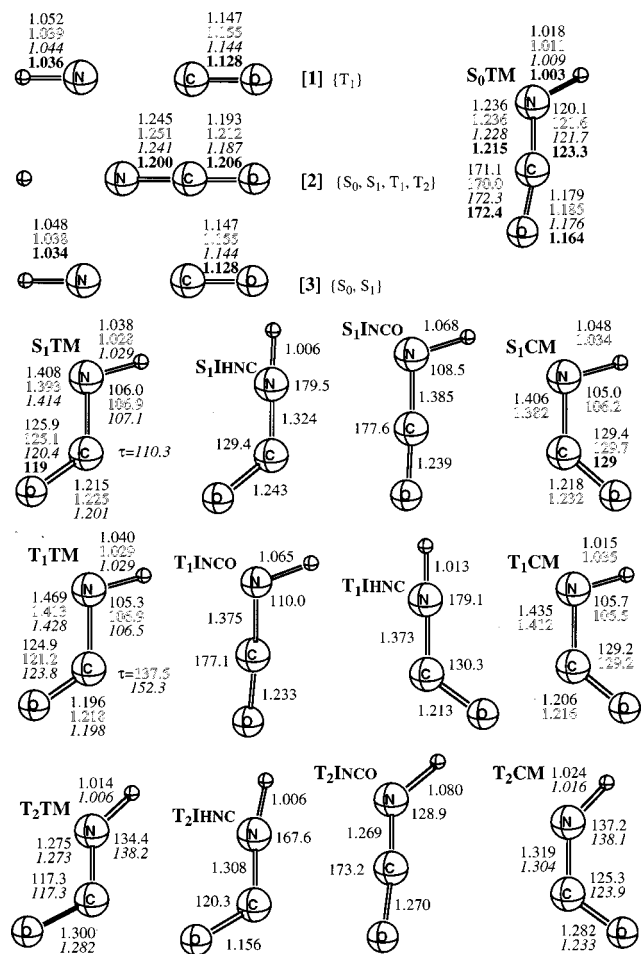


FIG. 1. Geometries (in Å and deg) of fragments and stationary points of HNCO on the four PES's. Plain numbers correspond to CASSCF, hollow to PT2-86, italics to CCSD/EOMCC, and bold to experiment. The states connected adiabatically to these fragment channels are shown in curly brackets. References for the experimental values are as follows. Channels [1] and [3]: Ref. 51. Channel [2]: Ref. 52. S_0 TM: Ref. 53. S_1 TM and S_1 CM: Ref. 1.

results on dissociation fragments. The overall agreement with experiment, where available, is good as far as structures (bonds and angles) are concerned. Unfortunately, the energetics are only in fair agreement with experiment. The most disconcerting discrepancy occurs for channel [1] energy. The calculated PT2-FV value underestimates the energy by 8 kcal/mol. The agreement is better for the higher-lying channels. These errors for channel energetics should provide an estimate for error bounds on the global potential energy surfaces. Thus, we expect the energy error associated with our CASPT2 methods to stay within 2–8 kcal/mol region. The CASSCF error may vary more, and we will try to avoid relying on the CASSCF energetics.

The transition states and minima are labeled according to the symmetry of the electronic state, the geometry of the structure, the number of imaginary frequencies (Nimag) at that geometry (**M** for Nimag=0 and **T** for Nimag=1), and the dissociation channel number, if any. Thus, S_1 CM indicates the *cis*-minimum on the S_1 surface whereas T_1 TT2 indicates the *trans*-transition state on the T_1 surface that leads to dissociation to channel [2]. Isomerization transition states have similar naming, i.e., the state, the indicator **I** of

isomerization TS, and the coordinate about which the isomerization occurs. For example, T_1 I_{HNC} means isomerization TS on T_1 via HNC rotation.

A. Stable structures and isomerization transition states on S_0 , S_1 , T_1 , and T_2 PES's

Optimized geometrical parameters of minima as well as isomerization transition states on various states are summarized in Fig. 1. Their energies are given in Table II. All the energies reported are relative to the global minimum on S_0 PES, S_0 TM, unless mentioned otherwise.

The S_0 PES. The global minimum of HNCO on the S_0 PES, S_0 TM, has an almost linear NCO moiety and connects to channels [2] and [3]. Its most important valence electronic configuration is

$$(4a')^2(5a')^2(6a')^2(7a')^2(1a'')^2(8a')^2(9a')^2 \\ \times (2a'')^2(10a')^0$$

in the order of increasing energy. The highest occupied MO (HOMO), $2a''$, is the out-of-plane π orbital with a high density on the nitrogen, and the lowest unoccupied MO (LUMO), $10a'$, is the CO in-plane π^* orbital. The present CASSCF, PT2-86, and CCSD structures agree well with experimental and previous theoretical results. Although other isomers of HNCO on S_0 exist,²⁶ they are separated from S_0 TM by high barriers and are not considered in the present study of isocyanic acid photodissociation.

The S_1 PES. This PES also connects to channels [2] and [3] and is one of the targets of our investigation since the initial stages of dissociation dynamics take place on the first excited singlet. Initially prepared on S_0 , the system is promoted by a UV photon to the lowest optically accessible electronic state, S_1 . The character of $S_1 \leftarrow S_0$ excitation is represented by $2a'' \rightarrow 10a'$ one-electron promotion and involves significant changes in geometry. As shown in Fig. 1, the CN bond stretches appreciably, and the NCO angle shrinks leading to either *cis* or *trans* isomers on the S_1 surface. At the PT2-FV//PT2-86 level, the planar S_1 TM and S_1 CM lie 84.7 and 88.2 kcal/mol, respectively, above S_0 TM. The *trans* isomer is 3.5 kcal/mol more stable than the *cis* isomer. Our previous MRSDCI calculations²⁹ also showed that the *trans* isomer is about 4 kcal/mol lower than the *cis*. The lower of the two minima, S_1 TM, is bound with respect to channel [2] by 24.0 kcal/mol and to channel [3] by 36.1 kcal/mol at the PT2-FV//PT2-86 level, which are deviated only as much as 1 kcal/mol from our previous MRSDCI results,²⁹ 23.3 and 37.1 kcal/mol, respectively.

Constrained to C_s symmetry, S_1 TM and S_1 CM are connected via two rotational isomerization transition states, S_1 I_{HNC} and S_1 I_{NCO}, whose energetics at PT2-86 level are 114.7 and 129.9 kcal/mol, respectively. PT2-FV puts the lower of the two, S_1 I_{HNC}, at 117.2 kcal/mol. These isomerization transition states represent the in-plane rotation of the HN and CO bonds, respectively. The lower of the two may play an important role in dissociation dynamics, as will be discussed later. The numerical PT2-86 geometry optimizations were very inefficient for isomerization transition states,

TABLE II. Energies of stable structures and isomerization transition states (in kcal/mol, with respect to the minimum on the ground state, S_0 TM), calculated with various methods.

Method											
Structure	CASSCF	PT2-FV	PT2-86	PT2-FV //PT2-86	EOMCC	EOMCC w.ZPE	MRSDCI Ref. 29	CASSCF Ref. 29	B3LYP Ref. 26	B3LYP w.ZPE Ref. 26	Expt. Ref. 31
S_1 TM	90.8		82.0	84.7	81.6	79.8	86.1	87.3			83-93
S_1 CM	93.0	88.8	86.3	88.2			90.1	92.1			
S_1 I _{HNC}	127.2	117.2	114.7				120.0	120.8			
S_1 I _{NCO}	133.8		129.9				131.9	134.4			
T_1 TM	84.0	79.2	75.6		77.5	75.6			84.6	82.6	
T_1 CM	91.4	85.5	81.4						85.2	83.1	
T_1 I _{HNC}	120.0										
T_1 I _{NCO}	134.5										
T_2 TM	106.6				95.5	99.2					
T_2 CM	99.4	90.4			90.4						
T_2 I _{HNC}	108.5	98.0									
T_2 I _{NCO}	151.6										

and so we only report CASPT2 single point energies at optimized CASSCF geometries for such structures.

We applied EOM-CC method to optimize several structures in out-of-plane geometries. Figure 1 also compares EOM-CC, CASSCF, and PT2-86 structures of minima, and their energetics are given in Table II. EOM-CC/D95++(d,p) calculations suggest that S_1 TM and S_1 CM are not stable in C_s symmetry and both lower their energy and converge towards a 110° dihedral angle structure, labeled S_1 TM- C_1 . Without zero-point vibrational energy (ZPVE), S_1 TM- C_1 is at 81.6 kcal/mol, 3 kcal/mol lower than the PT2-FV//PT2-86 C_s value. With ZPVE this minimum is at 79.8 kcal/mol. Here, the most disturbing discrepancy is that S_1 TM and S_1 CM are stable with respect to out-of-plane motion at CASSCF and PT2-86 levels of theory while they are unstable at the EOMCC level. An additional EOMCC calculation with a larger basis set, *cc*-PVTZ,⁴³ at the geometry optimized with EOMCC/D95++(d,p) constrained to C_s , showed that both *cis* and *trans* planar isomers are actually stable with respect to small torsional displacements. Furthermore, single point EOMCC/PVTZ calculation at the geometry optimized at EOMCC/D95++(d,p) level destabilized S_1 TM- C_1 by 7 kcal/mol unraveling a very inconsistent behavior of the EOMCC method. Therefore, we will try to rely only on PT2-FV and PT2-FV//PT2-86 energetics, and CASSCF and PT2-86 geometries in the discussion of dissociation dynamics. An experimental assignment of S_1 minimum including ZPVE is ~ 93 kcal/mol,³¹ as shall be discussed later.

The T_1 PES. This PES, connecting channels [1] and [2], has been investigated extensively by Mebel and co-workers using density functional theory.²⁶ T_1 comes from the same electronic excitation as S_1 but with a spin-flip. At PT2-FV level the lowest planar isomers are T_1 TM and T_1 CM being 79.2 and 85.5 kcal/mol above the ground minimum. Their structures are very similar to the corresponding S_1 structures, since both states have the same most important electronic configuration ($2a''$)($10a'$). As is also expected, the triplet is slightly lower in energy than the singlet for the corresponding isomer.

Mebel *et al.* found two nonplanar *cis* and *trans* isomers

at 71.8 and 71.2 kcal/mol, respectively, with a very low isomerization barrier connecting the two structures. It was found that the inclusion of ZPVE put the isomerization transition state below the ground vibrational level and smeared out the vibrational wave function over the two isomers, and the existence of two distinct structures was purely symbolic. PT2-86 geometry optimizations showed that T_1 TM was nonplanar with the dihedral angle of 137° , while T_1 CM was found to be planar. Unfortunately, the geometry of the connecting barrier could not be determined due to convergence problems in geometry optimizer. Based on Mebel's DFT results, we presume that this barrier is small.

Similar to the planar singlets, the triplet C_s isomers are connected by rotational transition states, T_1 I_{HNC} and T_1 I_{NCO}, with CASSCF energies of 120.0 and 134.4 kcal/mol. However, as maintained above, neither is thought to be the lowest transition state for isomerization and will not be further discussed in this section.

The T_2 PES. The higher-lying triplet is T_2 , whose most important electronic configuration is ($9a'$),($10a'$), achieved by a $9a' \rightarrow 10a'$ one-electron excitation from S_0 , where $9a'$ is qualitatively an in-plane π -type orbital of NO. T_2 connects channel [2] and $\text{HN}(A^3\Pi) + \text{CO}$. Two planar isomers, T_2 TM and T_2 CM, were found on this PES. Their CASSCF energies are 106.6 and 99.4 kcal/mol, respectively. PT2-FV gives the energy of the more stable isomer at 90.4 kcal/mol. A very low isomerization transition state was found to connect the two minima. Similar to S_1 and T_1 , it represents the hydrogen rotation about the CN bond. Labeled T_2 I_{HNC}, it lies only 2 kcal/mol above the higher, *trans* isomer at CASSCF level. Also found was an oxygen rotation transition state, T_2 I_{NCO}, appearing much higher than T_2 I_{HNC}. The importance of the lower transition state will be addressed in the discussion section.

B. Transition states on T_1 for N-C bond fission into $\text{HN}(X^3\Sigma^-) + \text{CO}$, channel [1]

The structures of the optimized transition states for bond fission channels are shown in Fig. 2. Their energies are summarized in Table III.

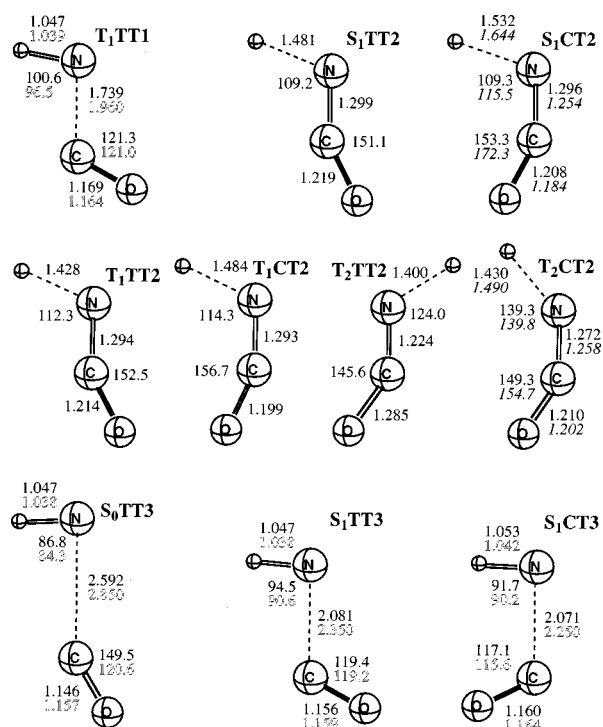


FIG. 2. Geometries (in Å and deg) of dissociation transition states for channels [1], [2], and [3]. Plain numbers correspond to CASSCF, hollow to PT2-86 and italics to CCSD/EOMCC. The dashed lines indicate the bonds being broken.

Previously, only a few theoretical studies reported the channel [1] dissociation transition state on the T_1 surface.^{26,44,45} Mebel *et al.*,²⁶ for example, calculated the barrier height to dissociation of 10.1 kcal/mol, and the reverse barrier of 4.4 kcal/mol, at the B3LYP/6-311G(*d,p*) level of theory. The present CASSCF estimate of T_1TT1 relative energy is 87.2 kcal/mol, which gives the forward barrier of 3 kcal/mol and the reverse barrier of over 20 kcal/mol. The transition state, T_1TT1 , has an elongated CN bond, but the other parameters do not change much compared to the planar T_1TM . PT2-86 changes CASSCF estimates drastically locating the energy of T_1TT1 at 83.4 kcal/mol yielding the forward barrier at 7.8 kcal/mol and the reverse at 5.8 kcal/mol. Here, PT2-86 agrees favorably with the B3LYP results.

C. Transition states on S_0 and S_1 for N–C bond fission into $HN(a^1\Delta) + CO$, channel [3]

The ground state S_0 PES exhibits a dissociation transition state, S_0TT3 , whose energy at CASSCF level is 110.7 kcal/mol, with a reverse barrier of only 0.8 kcal/mol. This is a very late transition state with CN bond of 2.5 Å, indicative of long-range $HN(a^1\Delta) \cdots CO$ interactions. A van der Waals structure may exist after the barrier, but we did not search for one. Despite the presence of the small barrier at CASSCF level, PT2-FV//PT2-86 shows that there is no distinguishable exit barrier on S_0 to channel [3]. The fact that this TS is so low, or nonexistent, will prove to be important in understanding the dissociation process.

Two dissociation transition states have been found on S_1 PES, namely, S_1TT3 and S_1CT3 . Stevens *et al.*²⁹ estimated the reverse barrier height at the lower S_1TT3 to be between 1 and 2 kcal/mol. Klossika *et al.*³⁰ derived the reverse barrier of ~ 1.4 kcal/mol. From PT2-86 calculation we also conclude that it should be slightly above 1 kcal/mol, as shown in Table III. S_1CT3 is predicted to be ~ 3 kcal/mol higher than S_1TT3 . The CN bond is approximately 2 Å, suggesting an earlier exit barrier on the S_1 PES, in contrast to the very late barrier at S_0TT3 . Experimental assignment of the reverse barrier height is 1.3 kcal/mol.^{23,42}

D. Transition states on S_0 , S_1 , T_1 , and T_2 for H–N bond fission into $H+NCO(X^2\Pi)$, channel [2]

This dissociation channel, open for all the four electronic states, is rich with transition states. The S_1 surface has two HN bond fission transition states, S_1TT2 and S_1CT2 , located in C_s at 130.7 and 117.4 kcal/mol, respectively, at PT2-86 level. It has been shown before that the *cis* exit barrier is substantially lower than *trans*.^{29,30} This conclusion is consistent with the present calculation. PT2-FV calculation puts the lower of the two transition states ~ 2 kcal/mol above the PT2-86 energy, yielding the reverse barrier of 11.3 kcal/mol. This estimate of the reverse barrier height agrees well with Klossika *et al.*³⁰ value of 12.9 kcal/mol, but it is several kcal/mol lower than Stevens *et al.*²⁹ estimate. The two transition states are characterized by an elongated HN bond, ~ 1.5 Å, which is significantly longer than the free HN bond. The NCO angle increases appreciably, indicative of NCO free

TABLE III. Energies of dissociation transition states (in kcal/mol, with respect to the minimum on the ground state, S_0TM), calculated with various methods.

Method	Transition State					EOMCC w.ZPE	MRSDCI Ref. 29	CASSCF Ref. 29	B3LYP Ref. 26	B3LYP w.ZPE Ref. 26	Expt. Ref. 42
	Structure	CASSCF	PT2-FV	PT2-86	PT2-FV //PT2-86						
T_1TT1	87.2		83.4						96.6	92.7	
S_1TT2	134.1		130.7				142.0	140.4			133.0
S_1CT2	122.8	119.6	117.4			129.7	126.7	130.0			
T_1TT2	134.1		128.3								
T_1CT2	121.3		116.3							121.4	114.7
T_2TT2	149.2		141.4								
T_2CT2	127.8		116.9			129.4		123.7			
S_0TT3	110.7										
S_1TT3	117.7		119.0	120.8							123.6
S_1CT3	121.8		122.0	124.1							

radical formation. The CASSCF geometries are in good agreement with Stevens *et al.* smaller scale CASSCF calculations. EOMCC, on the other hand, yields the CN bond 0.1 Å longer and the NCO angle 20° larger, indicative of a later transition state.

The T_1 PES also exhibits two dissociation transition states, T_1TT2 and T_1CT2 , with geometries very similar to those of S_1 . The CASSCF energy of the *cis* structure is very close to the result of Mebel *et al.*²⁶ At PT2-86 level the respective energies for the two transition states are 128.3 and 116.3 kcal/mol and the reverse barrier heights are 28.5 and 16.5 kcal/mol, respectively.

Finally, we have found two dissociation transition states on T_2 surface, T_2TT2 and T_2CT2 . Structurally, the T_2 transition states differ from S_1 or T_1 conformation by a larger HNC angle and a slightly shorter CN bond, as seen in Fig. 2. PT2-86 does not significantly change the overall qualitative picture of the CASSCF energetics. T_1CT2 is the lowest barrier to channel [2] with T_2CT2 being only 0.6 kcal/mol above it, followed by S_1CT2 0.5 kcal/mol higher. The reverse barrier heights at PT2-86 level are 41.6 and 17.1 kcal/mol for the respective T_2 structures.

No dissociation transition state was found on the S_0 surface. The dissociation pathway is energetically uphill all the way to the dissociation product. This result is consistent with recent experimental observations on channel [2] product energy distribution.⁴²

E. Minima of the seam of crossing between PES's

The electronic states presented here were obtained as eigenstates of the adiabatic, Born–Oppenheimer basis. Thus, the electronic wavefunction is allowed to change character, i.e., mix with other states, depending on the nuclear coordinates. Such mixing often results in radiationless transitions from upper to lower adiabatic state. The probability of such a transition depends on the relative energies of the two states, their gradients and magnitude of the nonadiabatic coupling element between the PES's. A perturbation treatment suggests that the transition is dominated by the crossing, i.e., when the two PES's have the same energy. In nonrelativistic treatment, states of same multiplicity are coupled via the derivative coupling term,⁴⁶ while states of different multiplicity are not coupled. However, in relativistic treatment, different multiplicities can couple via the spin–orbit operator.⁴⁷ For first row elements, the spin–orbit interaction is very small, resulting in a coupling element being much smaller than the derivative coupling term. Therefore, in the present system, we treat the S_0/S_1 and T_1/T_2 couplings, better known as the internal conversion (IC), as much more efficient nonadiabatic transitions than the S_i/T_j couplings, known as the intersystem crossing (ISC).

The seam of crossing between two states with the same space and spin symmetry can occur in up to $3n-8$ dimensions, while that between states with different space or spin symmetry occurs in up to $3n-7$ dimensions, where n is the number of atoms in the system. The lowest point on the seam of crossing hypersurface (MSX) is a critical point which gives the minimum energy required (neglecting tunneling) to make transition between the two states. The MSX also has a

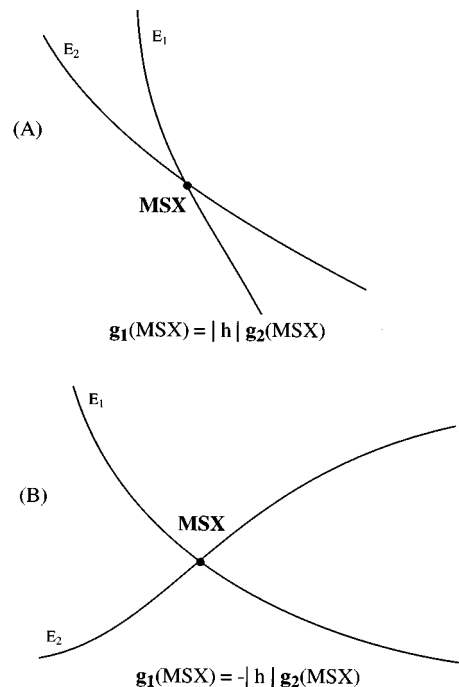


FIG. 3. Schematic 1D representation of two states crossing. Assuming that the crossing point (shown by the dot) is an MSX, the two gradients are parallel (A) or antiparallel (B).

property, where the energy gradients (the negatives of the forces) of the two crossing states are proportional, i.e., $g_2 = hg_1$.⁴⁸ If h is positive, the two gradient vectors are parallel, i.e., the two PES's cross like Fig. 3(A) in the 1D cut along the energy gradient. If h is negative, the two gradients are antiparallel and the two PES's cross like Fig. 3(B). The most important consequence of these gradient relations is that a nonadiabatic transition should be more favorable for parallel gradients than for antiparallel due to the simple 1D arguments of the Landau–Zener model. We located MSX's between the states of our interest with the SEAM⁴⁹ code employing CASSCF energies and gradients as well as those of EOMCC. At the CASSCF and EOM-CCSD geometries, spin–orbit coupling matrix elements between a singlet and a triplet were calculated with the smaller CASSCF using GAMESS96.

The optimized MSX structures and the gradient vectors, g_2 and g_1 , are shown in Fig. 4. Their energies and key geometrical parameters are shown in Table IV.

S_0/S_1 seam. The S_0/S_1 seam is easier to find in planar geometries where it allowed by symmetry. Using S_1TT3 geometry as a starting guess, CASSCF yielded the S_0/S_1 MSX structure, S_0S_1TX , with a very elongated CN bond of 2.57 Å, as shown in Table IV. In fact, the MSX was found with the C–N separation that was larger than that of S_0TT3 . This MSX was somewhat concerning because it is almost in the asymptotic region. As a measure of qualitative correctness, we performed a series of 2D PT2-86 scans, with only the CN and NCO coordinates varied while the other parameters were fixed at S_1TM . The approximate MSX floated well inside all the channel [3] exit barriers on S_0 and S_1 with the CN bond of 1.9 Å. The calculated crossing point was located energeti-

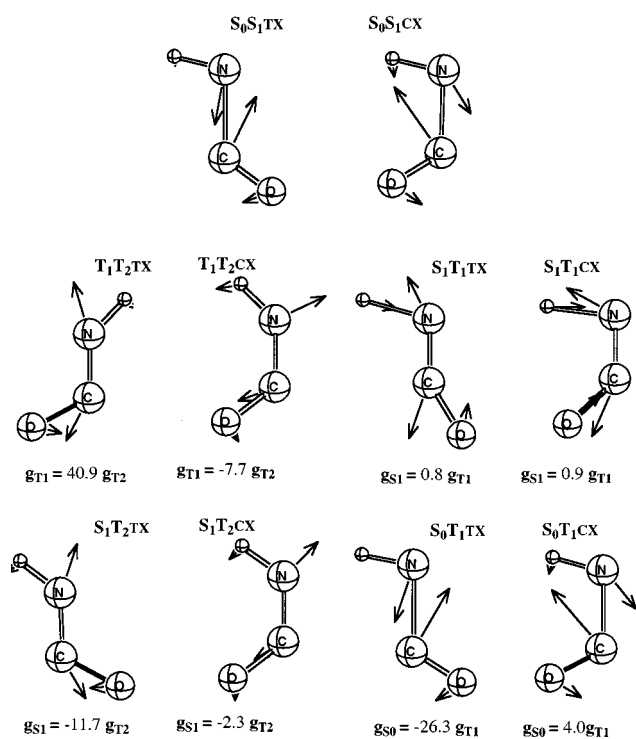


FIG. 4. CASSCF energy gradients (shown by arrows) at minima on seams of crossing (MSX's). For the T_1T_2TX , for instance, the gradient for the first state T_1 is shown in the figure, and the relationship between T_1 and T_2 gradients is given by an equation. For S_0S_1 MSX's which are not fully optimized (see text), the EOMCC gradient on the S_0 state is shown.

cally near channel [2] threshold. The more accurate CCSC (S_0)/EOMCC(S_1) surface crossing determination found two S_0/S_1 approximate MSX structures (we could not converge exactly to an MSX due to multireference character of S_0 and consequent failure of CCSD). The *trans* MSX structure S_0S_1TX is lower than the *cis* S_0S_1CX and is located at 89.4 kcal/mol and well below channels [2] and [3]. The CN bond for both of these MSX's is relatively short, ~ 1.7 Å.

As a consequence of nonconverged MSX, the gradients of the two states for either *cis* or *trans* were not

(anti-)parallel. Nevertheless, they appeared aligned, suggesting a close presence of the true MSX. The S_0 gradient was found to be about an order of magnitude larger than that of S_1 . It points towards shortening the CN bond and straightening the NCO moiety.

We did not attempt to find S_0/S_1 crossing with a stretched HN bond since S_0 does not have a barrier, while S_1 shows high barrier along this coordinate. Similarly, we did not search extensively in the Franck–Condon region as the two states are expected to be far apart energetically. In fact, we believe that S_0S_1TX and S_0S_1CX are the only low-lying MSX's in the energy region available after 217–230 nm photoexcitation.

As soon as the molecule breaks the planar symmetry, the two singlet states will avoid crossing, resulting in a symmetry-allowed conical intersection. Formally, the upper sheet of the conical intersection should be S_1 , and the lower should be S_0 , but since all the MSX's found here were constrained to C_s symmetry, the original labeling will be retained.

T_1/T_2 MSX. The other case of internal conversion that was considered is T_1/T_2 coupling. Once again, the search for the MSX was constrained to planar geometries to ensure a symmetry allowed crossing. T_1/T_2 *trans* seam of crossing, T_1T_2TX , was found near the *trans* minimum on T_2 PES; in fact, the MSX is very similar to T_2TM for both CASSCF and EOMCC. T_1T_2CX could not be found with CASSCF, but was located with EOMCC at 4 kcal/mol below T_1T_2TX . Both MSX's are in the Franck–Condon region and occur below channels [2] and [3]. Similarly to S_0/S_1 , we continue to use the original labeling of states.

S_0/T_1 MSX. Intersystem crossings were calculated in a similar manner. Minima on seams of crossing were located with CASSCF and EOMCC while spin–orbit coupling was calculated using the small-scale CASSCF wave function. S_0/T_1 seam of crossing has been investigated before.²⁶ The MSX was identified to occur before T_1TT1 and 2.5 kcal/mol (ZPE included) below channel [1]. CASSCF presented here locates the MSX just past the TS on the triplet surface and at the same energy as T_1TT1 (~ 23 kcal/mol) above channel

TABLE IV. Energies (in kcal/mol, with respect to the minimum on the ground state, S_0TM) and geometries (in Å and deg) of MSX's calculated with various methods. CCSD/EOMCC numbers appear in italics.

Structure	CASSCF	EOMCC	H–N	N–C	C–O	HNC	NCO
S_0S_1CX		95.6	1.045	1.628	1.173	101.8	124.6
S_0S_1TX		89.4	1.036	1.755	1.160	105.0	126.0
T_1T_2CX	102.4		1.004	1.336	1.224	134.9	126.7
T_1T_2TX		91.5	1.021	1.324	1.226	128.9	126.4
T_1T_2TX	106.6		1.014	1.274	1.300	135.4	117.1
T_1T_2TX		95.6	1.007	1.275	1.282	135.7	117.8
S_0T_1CX	91.2		1.047	1.590	1.191	102.6	120.7
S_0T_1TX	87.2		1.047	1.749	1.168	100.4	121.7
S_0T_1TX		81.9	1.035	1.577	1.189	103.8	115.9
S_1T_1CX	118.5		1.349	1.298	1.308	97.4	133.5
S_1T_1TX	130.0		1.369	1.294	1.265	105.0	148.6
S_1T_2CX	100.9		1.031	1.334	1.229	126.0	127.2
S_1T_2CX		93.6	1.025	1.328	1.222	122.9	128.5
S_1T_2TX	106.7		1.016	1.279	1.298	131.4	118.2
S_1T_2TX		96.1	1.010	1.283	1.275	130.9	119.3

[1]. EOMCC lowers the energy of S_0T_1TX by 5 kcal/mol and shortens the CN bond by almost 0.2 Å. CASSCF located S_0T_1CX at 91 kcal/mol with a somewhat shorter CN bond. S_0T_1CX was not found with EOMCC. Spin-orbit coupling element at the geometry shown in Table IV is ~ 15 cm $^{-1}$.

S_1/T_1 MSX. Other important intersystem crossings involve S_1/T_1 coupling. There were located two minima on S_1/T_1 seam of crossing with CASSCF: S_1T_1CX and S_1T_1TX . The lower of the two, S_1T_1CX , is 118.5 kcal/mol above the global minimum and is characterized by elongated HN and CO bonds. At CASSCF level it occurs below all the barriers to channel [2] but above channel [3]. Its counterpart, S_1T_1TX , is significantly higher in energy, has shorter CO bond but slightly longer HN bond. The magnitude of spin-orbit coupling for these two structures is of the order of 1 cm $^{-1}$. Note that S_1/T_1 coupling is much weaker than S_0/T_1 . These MSX's were not located with EOMCC as the two states climbed high on the repulsive wall of the CN bond but never approached each other closer than ~ 1 kcal/mol.

S_1/T_2 MSX. S_1/T_2 intersystem crossing has also been studied. Two distinct minima of crossing, S_1T_2CX and S_1T_2TX , were found with CASSCF on S_1/T_2 seam of crossing. Both of these structures are very similar to the corresponding minima, T_2CM and T_2TM . The two MSX's were found with EOM-CC as well; their respective energies are 94 and 96 kcal/mol. Spin-orbit coupling calculations showed that the strength of interaction of S_1 and T_2 at the MSX's, ~ 39 cm $^{-1}$, is much larger than S_1/T_1 and comparable to that of S_0/T_1 .

IV. DISCUSSIONS WITH COMPARISON TO EXPERIMENT

A. One photon excitation of ground state S_0 : The $S_1 \leftarrow S_0$ spectrum

Up to date there is no well-established experimental value of the energy of the S_1 minimum. Reisler and co-workers, for example, estimate the upper bound to be ~ 100 kcal/mol.⁵⁰ A more recent experimental study by Crim and co-workers²⁵ addressed the excitation spectrum of $S_1 \leftarrow S_0$ in more detail. The lowest transition that they observe directly is 94.6 kcal/mol.³¹ It should be mentioned that they find a yield of channel [1] products at this excitation energy. However, they estimate the band origin, i.e., the energy of the $S_1(v=0) \leftarrow S_0(v=0)$ transition, to be 92.8 kcal/mol,³¹ based on a simulation of spectral peak progressions. Such a difference between observed and simulated transition energies is understandable in view of the fact that the 0–0 transition should be very weak due to a poor Franck–Condon overlap between S_0 and S_1 vibrational wave functions, caused by very different geometries of S_0 and S_1 minima. Our best theoretical estimate of the band origin is 89.8 kcal/mol [to the planar S_1TM at the PT2-FV/(avtz w/o diffuse df)//PT2-86 level without ZPVE], and 87.6 kcal/mol with ZPVE [ZPVE at EOMCC D95++(d) level for S_0 and S_1] compared with the previous value of 86.1 of Stevens *et al.*²⁹ We suspect that at present our *ad hoc* method largely underestimates the true band origin, but our key conclusion is that the first observed peak of the spectrum is not the ground vibra-

tional minimum of S_1 ; it is, rather, some vibrationally excited mode. In the future we plan to solve for exact bound vibrational states and perform assignment of the spectrum.

Previously it was found that the electronic dipole transition moment is very much geometry dependent with strong preference towards *trans* conformations.²⁹ The present small-scale CASSCF calculations agree with this conclusion; after excitation the system will most likely end up in a *trans* geometry on S_1 with not only strongly bent NCO angle, but also with a stretched CN bond. Nonetheless, there will be a strong competition between the electronic dipole transition moment and the vibrational wave function overlap (Franck–Condon factor). The detailed analysis of the vibrational levels on the S_1 state requires multidimensional PES and corresponding multidimensional vibrational wave functions. This will be the subject of a further study. Based on these theoretical results and experimental findings, we qualitatively conclude that, after excitation to S_1 at energies below [2] and [3] dissociation thresholds, the system is likely to be found in highly excited vibrational states in the *trans* part of the S_1 PES. At excitation energies around channel [3] threshold, i.e., slightly above the lower isomerization barrier on the S_1 surface, the system would still prefer the *trans* region, but the vibrational wave function would not be localized to this region and will sample *cis* configuration as well.

B. Photolysis near the channel [3] threshold

In this section, we will consider the mechanism of HNCO photodecomposition near the energy of channel [3] fragments. The potential energy profiles for pathways leading to channel [1], [2] and [3] are shown in Figs. 5(A), 5(B), and 5(C), respectively.

Direct dissociation to [2] on S_1 . Consider that starting from the ground vibrational level of S_0 , the system is promoted to highly vibrationally excited S_1 and has an energy near the channel [3] threshold. Having overcome the isomerization barrier $S_1I_{\text{HNC}} \sim 1700$ cm $^{-1}$, and having sampled *cis* configurations, HNCO may have enough energy to pass S_1CT2 . Even though this would lead to a direct dissociation on S_1 to channel [2], the experimentally estimated barrier is several kcal/mol higher.⁴² In addition, experimental implications are such that at the excitation energies being discussed, channel [2] decomposition time scales resemble more an internal conversion rather than direct S_1 dissociation. Moreover, two high-level *ab initio* calculations^{29,30} also place the S_1 exit barrier a few kcal/mol above the present PT2-FV estimate. Thus, at present, we will not insist that direct dissociation on S_1 to [2] is possible at the energies near channel [3] threshold. A more accurate calculation will be needed to answer this question unambiguously.

$S_1 \rightarrow S_0$ internal conversion and dissociation on S_0 to [2] and [3]. Instead of sampling the possibly energetically unavailable S_1 exit barrier to channel [2], the system may continue to evolve on S_1 , sample the regions where S_1 crosses S_0 and make an efficient nonadiabatic transition to S_0 . Two near minimum energy points of S_1/S_0 crossing hypersurface are S_0S_1TX and S_0S_1CX , as shown in Figs. 5(B), and 5(C). Clearly, the system has enough energy to reach the S_1/S_0 crossing hypersurface. Having made a transition to S_0 , the

system will find itself in a highly vibrationally excited state of S_0 with most of the energy stored in the CN stretch, as follows from the geometries and gradients of S_0S_1TX and S_0S_1CX in Table IV and Fig. 4. The S_0 gradient at the seam of crossing along the CN bond is attractive, much larger than and parallel to that of S_1 , and HNCO may readily, without a barrier, proceed on S_0 to form channel [2] products with the excess of 10 kcal/mol distributed in translation, vibration, and rotation of the products. The gradient on S_0 on the S_0/S_1 seam is such that the NCO part tends to straighten out giving little push to hydrogen, which would explain the small recoil anisotropy of hydrogen atom images.⁴² Disfavored by gradient and the smaller phase space but having the available energy, a smaller fraction of molecules will proceed to dissociate on S_0 into products [3] making up the smaller yield observed experimentally.

$S_1 \rightarrow [3]$ and its competition with $S_1 \rightarrow S_0 \rightarrow [3]$. Reisler and co-workers observed that at energies just above [3] threshold, the product recoil anisotropy of channel [3] fragments is very weak whereas at energies slightly exceeding the S_1 exit barrier to [3] the anisotropy of the products is substantially higher.⁴² We find that the lowest exit barrier on S_1 , S_1TT3 , is $\sim 430 \text{ cm}^{-1}$ above the asymptote, as shown in Fig. 5(C). The most reasonable explanation to this anisotropy effect is the competition of S_0 and S_1 surfaces. At energy below S_1TT3 , as discussed in the above paragraph, HNCO can only dissociate on S_0 to form channel [3] products previously having overcome IC. Since there is no barrier on S_0 and since IC impedes direct dissociation, the system will evolve slowly without appreciable torque. On the other hand, at energy just above S_1TT3 , the direct dissociation on S_1 wins the competition, and the system can fall apart very fast experiencing strong internal forces on the S_1 surface. This explanation is in accord with Reisler's argument.

Enhancement by initial HN stretch excitation: $S_1 \rightarrow T_1 \rightarrow [2]$ pathway. Crim and co-workers investigated the dependence of yield to channel [2] on the initial excitation of the HN stretch at total energies around channel [3] threshold.^{2,25} They found that the production of channel [2] fragments is enhanced by a factor of four compared to isoenergetic excitation with vibrationally cold HN stretch.

In view of the present calculations we can suggest the following two factors for explanation. (1) As argued before, both *cis* and *trans* configurations on S_1 surface can be sampled at the excitation energies near channel [3] threshold. Thus, the S_1/T_1 *cis* MSX (S_1T_1CX) should be available to the system (*trans* is too high). At this MSX the HN bond is significantly stretched, as seen in Table IV. The initial vibrational energy in the HN stretch will help the system to reach this MSX. (2) The gradient on T_1 at this MSX is strongly attractive along the HN bond and parallel to S_1 , as can be seen in Fig. 4, and even though the system is energetically above T_1CT2 , the attractive gradient may try to pull the system into the T_1 minimum and not allow to dissociate freely to channel [2] products. Hence, additional energy in the HN stretch would promote the system to the stretched HN bond region and provide the necessary push to dissociate HNCO into H and NCO. Even though S_1/T_1 electronic coupling is very weak (largely due to symmetry reasons), the

involvement of torsional degree of freedom may strengthen the interaction by lowering the symmetry of both wave functions.

Stevens *et al.* argued that if the N–H stretch energy is locked in that mode then S_1IHNC would probably be energetically unavailable for the reaction.²⁹ Although the initial H–N stretch on S_0TM , where NCO part is almost linear, is a good vibrational quantum number, it may become highly mixed with HNC and NCO angles on S_1 . Consequently, the energy is no longer locked in the HN mode and the system can easily access the S_1IHNC isomerization barrier and various MSX's in *cis* geometries. Some quantum or classical dynamics calculations are needed for more quantitative argument.

Competition between nonadiabatic pathways. After the efficient S_1/S_0 internal conversion, the system will compete between S_0/T_1 ISC and dissociation on S_0 . The energetically available S_0T_1TX is the minimum point on S_0/T_1 crossing space, and, in fact, it is very similar to T_1TT1 with a shorter CN bond. The gradient on T_1 , however, is much smaller than that of S_0 . The S_0T_1CX structure, on the other hand, has a much larger T_1 gradient, and it is parallel with S_0 . Also, the *cis* crossing point is only ~ 4 kcal/mol higher than the *trans* counterpart, so the system may prefer the *cis* configurations to make the transition. After the transition, it can proceed to dissociate to channel [1] with 40 kcal/mol in excess. But ISC is a much less probable occurrence than IC, and this is the reason why channel [1] products are observed at much smaller quantities than the other fragments. The proposed $S_1 \rightarrow S_0 \rightarrow T_1 \rightarrow [1]$ dissociation pathway is consistent with Reisler's findings.⁴² Based on product recoil anisotropy arguments, the authors suggest that there has to be an intermediate step in the $S_1 \rightarrow T_1 \rightarrow [1]$ pathway. Estimating the lifetime of the intermediate, they propose that it must be S_0 , which is clearly evident from our calculations. Intuitively, we can conclude that channel [1] products should appear at any initial excitation wavelength with almost a constant yield since channel [1] and S_0/T_1 crossing are located at relatively low energy. This conclusion is in agreement with the experimental observation on $HN(^3\Sigma^-) + CO$ products.²²

None of the MSX's involving S_1/T_1 , S_1/T_2 , S_0/T_1 , and T_1/T_2 couplings has strong repulsive gradient on T_1 along the HN bond. This situation is likely to cause a competition between channel [2] and channel [1] dissociation on T_1 . Examination of the T_1 gradient of S_1/T_1 , S_0/T_1 , and T_1/T_2 seams of crossing shows that it is repulsive along the CN coordinate, which produces a strong drive towards channel [1] products. Hence, $S_1 \rightarrow T_1 \rightarrow [1]$, $S_1 \rightarrow T_2 \rightarrow T_1 \rightarrow [1]$, and $S_1 \rightarrow S_0 \rightarrow T_1 \rightarrow [1]$ will dominate nonadiabatic dissociation unless the HN mode is excited. Thus, we believe that when Crim and co-workers prepare S_0 initially excited in the HN mode, they predetermine efficient dissociation to channel [2] and automatically reduce the yield of channel [1] products. This reduction, however, should be relatively small as the main path for channel [1] is expected to be the S_0/T_1 intersystem crossing. In addition, the ratio of yields [2]/[3] is expected to be greater than unity for the excitation energy being discussed, due to the greater number of openings that lead to products [2] and electron spin statistics.

C. Photolysis at energy substantially exceeding channel [3]

At higher excitation energies the barriers to all the channels are exceeded. In this situation, a different type of channel competition should be expected. Since S_1 has a strong repulsive gradient along the CN bond and a small gradient along the HN bond, preference should be given to the direct dissociation on S_1 . In fact, as the excitation energy increases, the yield to channel [3] with a lower barrier will increase and that of channel [2] with a higher barrier will drop. As long as S_0/S_1 internal conversion remains efficient, the yield to channel [1] should not vanish. Very similar arguments were used in photofragment imaging experiments.²² In the present work we have not investigated the role of S_2 and the higher-lying exit channels. Obviously, they will become important at high excitation energies.

V. CONCLUSIONS

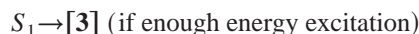
We used high level *ab initio* calculations, CASSCF and CASPT2, to investigate the complex process of isocyanic acid photodissociation dynamics. Results of several experimental studies are used as a guide to unravel the puzzle of competition for dissociation between three channels: $\text{HN}({}^1\Delta) + \text{CO}[3]$, $\text{H} + \text{NCO}({}^2\Pi)[2]$, and $\text{HN}({}^3\Sigma^-) + \text{CO}[1]$. Four distinct potential energy surfaces, S_0 , S_1 , T_1 , and T_2 , are involved in the process.

We confirmed that S_1 has a low reverse barrier of 1.2 kcal/mol to products [3] and a rather high reverse barrier of 11.3 kcal/mol to channel [2]. S_0 , on the other hand exhibited no barriers to either channel. Rather low reverse barriers on T_1 and T_2 were found to block products [2]. Numerous internal conversion coupling channels and intersystem crossings were located.

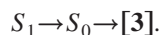
The question of the $S_1 \leftarrow S_0$ excitation spectrum has been briefly addressed. Based on the geometries of the minimum structures on S_0 and S_1 we conclude that the band origin should be very weak if present at all in the absorption spectra. Spectral simulations put the band origin ~ 2 kcal/mol below the lowest observed transition. Clearly, Franck-Condon factors disfavor the 0-0 transition.

Experimental findings of the channel [2] yield dependence on energy, which is partly supplied as HN vibration, are best explained in terms of the topology of the surfaces that lead to that channel. In the regions where the various surface coupling occur, the HN gradient is strongly attractive, and although the system may have enough energy to surpass an exit barrier, the gradient will impede the dissociation. Thus, any additional energy stored in the HN vibration will help promote the dissociation and increase the yield. Moreover, initial energy stored as HN vibration on the S_0 surface will very likely be redistributed among the two angular modes, HNC and NCO, owing to the strongly bent excited states geometries. Therefore, the initial energy stored in HN mode will also mediate isomerization and make surface crossings more available.

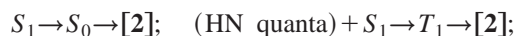
At photoexcitation energies near channel [3] threshold, products to channel [3] are suggested to be yielded via the following mechanisms:



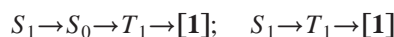
and



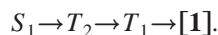
Channel [2] mechanism is substantially more involved:



Finally, the system is suggested to dissociate into channel [1] as follows:



and



At higher photoexcitation energies channel [3] is expected to be dominant while channel [2] is expected to drop rapidly. Products of channel [1] are expected to appear at any excitation wavelength.

ACKNOWLEDGMENTS

The authors are extremely grateful to Professor Hanna Reisler and Professor Fleming Crim for many stimulating discussions and for making experimental results available prior to publication. This work was in part supported by the Grants Nos. F49620-98-1-0063 and F49620-98-1-0345 (purchase of PC cluster) from the Air Force Office of Scientific Research, and Grant No. CHE 9810106 from the National Science Foundation. Acknowledgment is also made for support of computing time at Emerson Center of Emory University, National Center for Supercomputing Applications (NCSA) and Maui High Performance Computer Center (MHPCC).

¹R. N. Dixon and G. H. Kirby, *Trans. Faraday Soc.* **64**, 2002 (1968).

²S. S. Brown, R. B. Metz, H. L. Berghout, and F. F. Crim, *J. Chem. Phys.* **105**, 6293 (1996).

³S. S. Brown, H. L. Berghout, and F. F. Crim, *J. Chem. Phys.* **105**, 8103 (1996).

⁴M. Zyrianov, Th. Droz-Georget, A. Sanov, and H. Reisler, *J. Chem. Phys.* **105**, 8111 (1996).

⁵A. Sanov, Th. Droz-Georget, M. Zyrianov, and H. Reisler, *J. Chem. Phys.* **106**, 7013 (1997).

⁶Th. Droz-Georget, M. Zyrianov, H. Reisler, and D. W. Chandler, *Chem. Phys. Lett.* **276**, 316 (1997).

⁷R. A. Brownsword, T. Laurent, R. K. Vatsa, H.-R. Volpp, and J. Wolfrum, *Chem. Phys. Lett.* **258**, 164 (1996).

⁸B. Bohn and F. Stuhl, *J. Phys. Chem.* **97**, 4891 (1993).

⁹J. Zhang, M. Dulligan, and C. Wittig, *J. Phys. Chem.* **99**, 7446 (1995).

¹⁰S. S. Brown, H. L. Berghout, and F. F. Crim, *J. Chem. Phys.* **102**, 8440 (1995).

¹¹S. S. Brown, C. M. Cheatum, D. A. Fitzwater, and F. F. Crim, *J. Chem. Phys.* **105**, 10911 (1996).

¹²S. S. Brown, H. L. Berghout, and F. F. Crim, *J. Chem. Phys.* **106**, 5805 (1997).

¹³R. A. Brownsword, T. Laurent, M. Hillenkamp, R. K. Vatsa, and H.-R. Volpp, *J. Chem. Phys.* **106**, 9563 (1997).

¹⁴S. S. Brown, H. L. Berghout, and F. F. Crim, *J. Chem. Phys.* **107**, 8985 (1997).

¹⁵S. S. Brown, H. L. Berghout, and F. F. Crim, *J. Chem. Phys.* **107**, 9764 (1997).

¹⁶M. Zyrianov, Th. Droz-Georget, and H. Reisler, *J. Chem. Phys.* **110**, 2059 (1999).

- ¹⁷K. Uno, T. Hikida, A. Hiraya, and K. Shobatake, *Chem. Phys. Lett.* **166**, 475 (1990).
- ¹⁸R. A. Brownsword, T. Laurent, R. K. Vatsa, H.-R. Volpp, and J. Wolfrum, *Chem. Phys. Lett.* **249**, 162 (1996).
- ¹⁹M. Kawasaki, Y. Sato, K. Sato, Y. Matsumi, and S. H. S. Wilson, *Chem. Phys. Lett.* **251**, 67 (1996).
- ²⁰R. A. Brownsword, M. Hillenkamp, T. Laurent, R. K. Vatsa, and H.-R. Volpp, *J. Chem. Phys.* **106**, 4436 (1997).
- ²¹A. L. L. East, C. S. Johnson, and W. D. Allen, *J. Chem. Phys.* **98**, 1299 (1993).
- ²²Th. Droz-Georget, M. Zyrianov, A. Sanov, and H. Reisler, *Ber. Bunsenges. Phys. Chem.* **101**, 469 (1997).
- ²³M. Zyrianov, Th. Droz-Georget, and H. Reisler, *J. Chem. Phys.* **106**, 7454 (1997).
- ²⁴A. Sanov, Th. Droz-Georget, M. Zyrianov, and H. Reisler, *J. Chem. Phys.* **106**, 7013 (1997).
- ²⁵H. L. Berghout, S. S. Brown, R. Delgado, and F. F. Crim, *J. Chem. Phys.* **109**, 2257 (1998).
- ²⁶A. A. Mebel, A. Luna, M. C. Lin, and K. Morokuma, *J. Chem. Phys.* **105**, 6439 (1996).
- ²⁷W.-H. Fang, X.-Z. You, and Z. Yin, *Chem. Phys. Lett.* **238**, 236 (1995).
- ²⁸A. L. L. East, Ph.D. thesis, Selected theoretical studies of vibrational anharmonicity and thermochemistry, Stanford, 1994.
- ²⁹J. E. Stevens, Q. Cui, and K. Morokuma, *J. Chem. Phys.* **108**, 1452 (1998).
- ³⁰J.-J. Klossika, H. Flöthmann, C. Beck, R. Schinke, and K. Yamashita, *Chem. Phys. Lett.* **276**, 325 (1997).
- ³¹L. Berghout and F. F. Crim (private communication).
- ³²T. H. Dunning, Jr., *J. Chem. Phys.* **53**, 2823 (1970); **55**, 3958 (1971).
- ³³Diffuse exponents were taken from Gaussian94 library of basis sets, M. J. Frisch, G. W. Trucks, H. B. Schlegel, P. M. W. Gill, B. G. Johnson, M. A. Robb, J. R. Cheeseman, T. Keith, G. A. Petersson, J. A. Montgomery, K. Raghavachari, M. A. Al-Laham, V. G. Zakrzewski, J. V. Ortiz, J. B. Foresman, J. Cioslowski, B. B. Stefanov, A. Nanayakkara, M. Challacombe, C. Y. Peng, P. Y. Ayala, W. Chen, M. W. Wong, J. L. Andres, E. S. Replogle, R. Gomperts, R. L. Martin, D. J. Fox, J. S. Binkley, D. J. Defrees, J. Baker, J. P. Stewart, M. Head-Gordon, C. Gonzales, and J. A. Pople, Gaussian, Inc., Pittsburgh, PA, 1995.
- ³⁴H.-J. Werner and P. J. Knowles, *J. Chem. Phys.* **82**, 5053 (1985); P. J. Knowles and H.-J. Werner, *Chem. Phys. Lett.* **115**, 259 (1985); H.-J. Werner and W. Meyer, *J. Chem. Phys.* **74**, 5794 (1981).
- ³⁵H.-J. Werner, *Mol. Phys.* **89**, 645 (1996).
- ³⁶G. D. Purvis III and R. J. Bartlett, *J. Chem. Phys.* **76**, 1910 (1992).
- ³⁷J. F. Stanton and R. J. Bartlett, *J. Chem. Phys.* **98**, 7029 (1993).
- ³⁸K. Ishida, K. Morokuma, and A. Komornicki, *J. Chem. Phys.* **66**, 2153 (1977).
- ³⁹MOLPRO 96.4, H.-J. Werner and P. J. Knowles, University of Birmingham, U.K., 1998.
- ⁴⁰M. W. Schmidt, K. K. Baldrige, J. A. Boatz, S. T. Elbert, M. S. Gordon, J. H. Jensen, S. Koseki, N. Matsunaga, K. A. Nguyen, S. J. Su, T. L. Windus, M. Dupuis, and J. A. Montgomery, *J. Comput. Chem.* **14**, 1347 (1993).
- ⁴¹J. Gauss, W. J. Lauderdale, J. F. Stanton, J. D. Watts, and R. J. Bartlett, *Chem. Phys. Lett.* **182**, 207 (1991).
- ⁴²M. Zyrianov, Th. Droz-Georget, and H. Reisler, *J. Chem. Phys.* **110**, 2059 (1999).
- ⁴³T. H. Dunning, Jr., *J. Chem. Phys.* **90**, 1007 (1989).
- ⁴⁴K. Yokayama, S.-Y. Takane, and T. Fueno, *Bull. Chem. Soc. Jpn.* **64**, 2230 (1991).
- ⁴⁵M. L. Lin, Y. He, and C. F. Melius, *Int. J. Chem. Kinet.* **24**, 1103 (1992).
- ⁴⁶D. R. Yarkony, *J. Phys. Chem.* **100**, 18 612 (1996); D. R. Yarkony, *Rev. Mod. Phys.* **68**, 985 (1996).
- ⁴⁷B. A. Hess, C. M. Marian, and S. D. Peyerimhoff, in *Modern Electronic Structure Theory I*, edited by D. R. Yarkony (Uto-Print, Singapore, 1995); M. Peric, B. Engels, and S. D. Peyerimhoff, in *Quantum Mechanical Electronic Structure Calculations with Chemical Accuracy*, edited by S. R. Langhoff (Kluwer Academic, Netherlands, 1995).
- ⁴⁸S. Kato, R. L. Jaffe, A. Komornicki, and K. Morokuma, *J. Chem. Phys.* **78**, 4567 (1983).
- ⁴⁹K. Dunn and K. Morokuma, *J. Chem. Phys.* **102**, 4904 (1995); Q. Cui, K. Morokuma, and J. F. Stanton, *Chem. Phys. Lett.* **263**, 46 (1996).
- ⁵⁰M. Zyrianov, A. Sazonov, R. A. Beaudet, and H. Reisler (private communication).
- ⁵¹K. P. Huber and G. Herzberg, *Constants of Diatomic Molecules* (Van Nostrand Reinhold, New York, 1979).
- ⁵²P. Misra, C. W. Mathews, and D. A. Ramsay, *J. Mol. Spectrosc.* **130**, 419 (1988).
- ⁵³K. Yamada, *J. Mol. Spectrosc.* **79**, 323 (1980).